

PAPER

Antiferromagnetic skyrmion repulsion based artificial neuron device

To cite this article: Namita Bindal *et al* 2021 *Nanotechnology* **32** 215204

View the [article online](#) for updates and enhancements.



240th ECS Meeting ORLANDO, FL

Orange County Convention Center Oct 10-14, 2021



Abstract submission due: April 9

SUBMIT NOW

Antiferromagnetic skyrmion repulsion based artificial neuron device

Namita Bindal¹ , Calvin Ang Chin Ian², Wen Siang Lew² and Brajesh Kumar Kaushik^{1,*} 

¹ Department of Electronics and Communication Engineering, Indian Institute of Technology, Roorkee, 247667, India

² School of Physical and Mathematical Sciences, Nanyang Technological University, 637371, Singapore

E-mail: bkk23fec@iitr.ac.in

Received 25 October 2020, revised 9 January 2021

Accepted for publication 2 February 2021

Published 4 March 2021



CrossMark

Abstract

Magnetic skyrmions are potential candidates for neuromorphic computing due to their inherent topologically stable particle-like behavior, low driving current density, and nanoscale size. Antiferromagnetic skyrmions are favored as they can be driven parallel to in-plane electrical currents as opposed to ferromagnetic skyrmions which exhibit the skyrmion Hall effect and eventually cause their annihilation at the edge of nanotracks. In this paper, an antiferromagnetic skyrmion based artificial neuron device consisting of a magnetic anisotropy barrier on a nanotrack is proposed. It exploits inter-skyrmion repulsion, mimicking the integrate-fire (IF) functionality of a biological neuron. The device threshold represented by the maximum number of skyrmions that can be pinned by the barrier can be tuned based on the particular current density employed on the nanotrack. The corresponding neuron spiking event occurs when a skyrmion overcomes the barrier. By raising the device threshold, lowering the barrier width and height, the operating current density of the device can be decreased to further enhance its energy efficiency. The proposed device paves the way for developing energy-efficient neuromorphic computing in antiferromagnetic spintronics.

Keywords: antiferromagnetic, skyrmion, repulsion, neuron

(Some figures may appear in colour only in the online journal)

1. Introduction

Neuromorphic computing paradigm mimics the neurobiology present in the biological nervous system. The computing components of the human brain are neurons whose interconnections are known as synapses. Neuromorphic computing based on artificial neural network (ANN) has certain advantages over Von Neumann architecture based classical computing with regard to adaptability, massive parallelism, energy efficiency [1] and, tolerance to fault and variation [2]. With the proven success and effectiveness of neuromorphic computations in solving many problems, there has been a drive to build artificial neurons and synapses on a chip dedicated to performing these computations effectively. In past decades, neuromorphic computing was implemented using complementary metal oxide semiconductor (CMOS) technology [3–6]. But, the discrepancy between

computing units of the brain and architecture of CMOS transistors leads to higher energy and resource requirements for CMOS based neuromorphic computing [7]. Bridging this gap requires alternate devices where neural and synaptic functionality corresponds to the device's operation. In recent decades, advances have been made in nanotechnology research with the introduction of spintronic devices for implementing low power and high-density neuromorphic computing [8–11].

A magnetic spin texture, skyrmions, are topologically stable field configurations that appear as particle-like solutions [12]. Magnetic skyrmions emanate from the chiral interactions which are induced due to lack of inversion symmetry in crystal lattices and are known as Dzyaloshinskii–Moriya interactions (DMI) [13]. DMI energy is depicted as $H_{DM} = -D_{12} \cdot (S_1 \times S_2)$, where S_1 and S_2 are two atomic spins and D_{12} is the DMI vector between these two spins. There are two main types of topologically identical magnetic skyrmions where spins at its periphery are in the opposite direction to the spins present at the center [14].

* Author to whom any correspondence should be addressed.

Bloch skyrmions exist in the systems with bulk DMI. Meanwhile, Neel skyrmion is produced by the interfacial DMI. In contrast to magnetic bubbles, micrometer-sized magnetic domains which are stabilized by the dipole interactions [15], magnetic skyrmions have a much lower size (1–100 nm) [15, 16] and improved stability in virtue of DMI [13]. Additionally, the driving current density for skyrmions (order of 10^6 A m^{-2}) is lower than that for the magnetic domains (10^{11} A m^{-2}) [12]. Skyrmions have potentially easy control of their motion by ultra-low current densities making them remarkable candidates for future high-density data storage and information processing devices [12, 16–22]. In 2016, Woo *et al* demonstrated the stabilization of skyrmions and their current-driven motion in ferromagnets. The motion of a train of individual skyrmions at speeds exceeding 100 m s^{-1} by the current density of $5 \times 10^{11} \text{ A m}^{-2}$ is reported [16]. But, the motion of magnetic skyrmions in ferromagnetic (FM) materials uphold a complication of exhibiting a Magnus force originating from skyrmion topology acting perpendicular to the applied current [23]. The transverse motion of skyrmions to the current direction is known as the skyrmion hall effect. This leads to the risk of annihilation of FM skyrmions at the nanotrack edge. Besides, FM skyrmions are also susceptible to stray fields [24, 25]. Regardless of interesting physics around the Magnus effect, for many applications, zero skyrmion hall angle is preferred for high-speed applications. In antiferromagnetic skyrmion (AFM), the effective skyrmion hall angle is zero as equal and opposite forces are acting on the two sublattices of the AFM skyrmion resulting in a straight trajectory of the AFM skyrmion along with the applied current [23]. In contrast to FM skyrmion, AFMs are insensitive to stray fields. AFM skyrmions have highly increased velocity by the order of 10^2 m s^{-1} as compared to FM skyrmion [25]. A convincing interest behind investigating skyrmions in antiferromagnets is due to DMI which is crucial for the creation of skyrmion [25], is more commonly found in AFM rather than FM [23]. This brings about AFM skyrmions as an ideal information carrier owing to a favorable candidate for spintronic applications.

In this work, an AFM skyrmion based artificial neuron device is proposed. It exploits inter-skyrmion repulsion on a nanotrack with a high energy barrier. We first describe the behavior of the biological neuron [26] as well as analogous prerequisites of the suggested artificial neuron. Then, we show that the skyrmion–skyrmion repulsion [27] can be explored to implement an integrate-fire (IF) spiking neuron functionality with a tunable number of skyrmions acting like the analog membrane potential of the biological neuron. The IF functionality and related interpretations of the proposed AFM skyrmionic neuron device is demonstrated using micromagnetic simulations.

Skyrmions based devices being nanoscale size, robust and non-volatile are compatible with CMOS [28]. Therefore, our study facilitates the design and integration of magnetic skyrmions based devices with conventional CMOS circuitry and will encourage further experimental studies in this research direction [29–32]. Furthermore, future work on integrating the proposed neuron device with its synaptic device, and CMOS circuitry can form AFM skyrmion-based neuromorphic system. These systems are very energy efficient

Table 1. Key parameters in micromagnetic simulations.

| Parameters | Values |
|------------------------------------|--|
| Saturation magnetization M_S | -375 kA m^{-1} |
| Exchange stiffness A | $-6.59 \times 10^{-12} \text{ J m}^{-1}$ |
| Gilbert damping α | 0.005 |
| Spin polarization rate P | 0.4 |
| Magnetic anisotropy (on nanotrack) | $1.16 \times 10^5 \text{ J m}^{-3}$ |
| Non-adiabatic STT β | 0.5 |
| Interfacial DMI D_{ind} | $1.2 \times 10^{-3} \text{ J m}^{-3}$ |
| Elementary charge e | $1.6 \times 10^{-19} \text{ C}$ |

and fast [33], and can be implemented for image processing applications.

2. Methods

The micromagnetic simulations were performed using the MuMax3 software [34–36]. The magnetization dynamics is computed using Landau–Lifshitz–Gilbert (LLG) equation [37]. In the simulations, the nanostripe is set to be $2048 \times 240 \times 1 \text{ nm}^3$. A discretization of $0.418 \times 0.418 \times 0.418 \text{ nm}^3$ of each cell is used. The proposed AFM skyrmion-based artificial neuron device was simulated by solving LLG equation by using the material parameters (see table 1) for KMnF_3 [23]. For $K_u = 1.4 \times 10^5 \text{ J m}^{-3}$ in the energy barrier region, the width of the barrier is varied in a step size of 8.36 nm. For the energy barrier width of 100.32 nm, the K_u of the barrier region is varied in a step of $0.5 \times 10^5 \text{ J m}^{-3}$. These variations in the device are carried out to achieve the operation of the proposed device discussed in section 4.

3. Analogy between a biological neuron and the proposed artificial neuron device

The basic component of the human brain is a neuron. A neuron has a cell body known as soma and has root-like extensions called dendrites [38]. Here, we describe the biological neural network (figure 1(a)) as well as its corresponding ANN schematic (figure 1(b)). The biological neural network consists of a massive number of neurons (approximately 10^{11}) that are interconnected to each other via junctions known as synapses (approximately 10^{15}) [38, 39]. The most salient feature of neural function is the action potential.

Integrate-and-fire neuron is one of the earliest neuron model [40–43]. Ion current through the cell membrane occurs when neurotransmitters activate the ion channels in the cell. This current is a time-dependent current represented as $I(t)$. The insulating membrane of the cell has the charge ion concentration that determines the capacitance C . A neuron responds to the signal with a voltage spike called an action potential represented as V . A time representation of the neuron model is $I(t) = C_m dV_m/dt$ [44]. Whenever an input current is applied, membrane potential increases with respect to time until it reaches a certain threshold. After that, a neuron

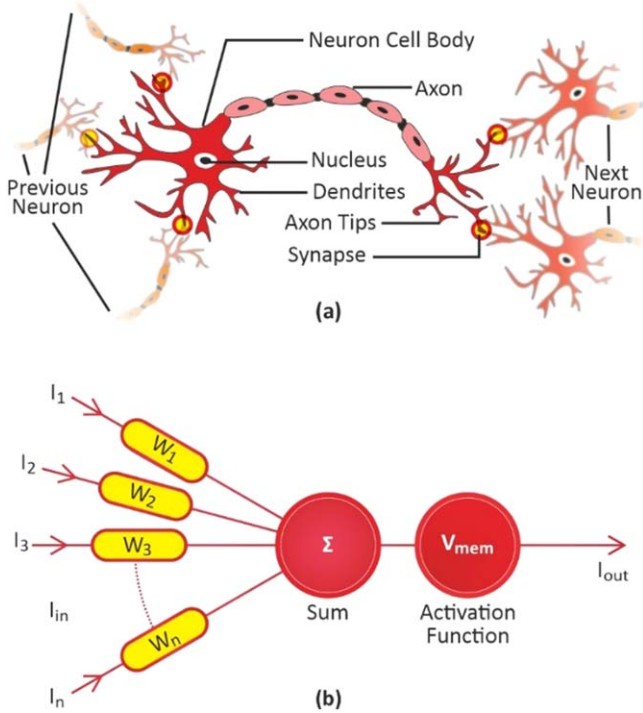


Figure 1. (a) Illustration of a biological neuron and the key components involved in information processing. (b) Corresponding artificial neural network.

will spike an output signal and then the voltage is reset to its resting potential.

Similar to the biological neural networks, the ANN is presented as a chain of spikes i.e. input signals from the neurons and pass the output signal to neurons connected to it based on the firing pattern specified to that particular neuron. Figure 1(b) illustrates the primary neuronal function. The equation $Y(t) = f(\sum w_i(t)I_i(t))$ defines the time-dependent neuron spike where f is the activation function such as sigmoid, linear, step, etc $w_i(t)$ and the $I_i(t)$ represents the synaptic weight and the input spikes of the i th synapse, respectively [45]. When the neuron receives the spikes from other associated neurons, there is a combination of membrane potential. However, only when the neuron membrane potential surpasses the specific threshold, the neuron will fire an output signal.

The biological neuron’s integrate and fire functionality is analogously described with the proposed AFM skyrmion-based artificial neuron device as shown in figure 2. In this device, the nucleation of skyrmions on the nanotrack is analogous to the input spikes of the neuron. The number of skyrmions present on the nanotrack is analogous to the membrane potential of the biological neuron. A pre-determined maximum number of skyrmions on the track is analogous to the threshold of the biological neuron. Once the threshold is reached, the device will trigger an output signal and reset. The snapshots of micromagnetic simulations in figure 2 show the IF behavior of the proposed device. Here, the AFM skyrmion is assumed to be nucleated with the 2 ns long pulse [25]. As the nucleation time for the skyrmion is non-zero, the delay is shown between the input spike and the

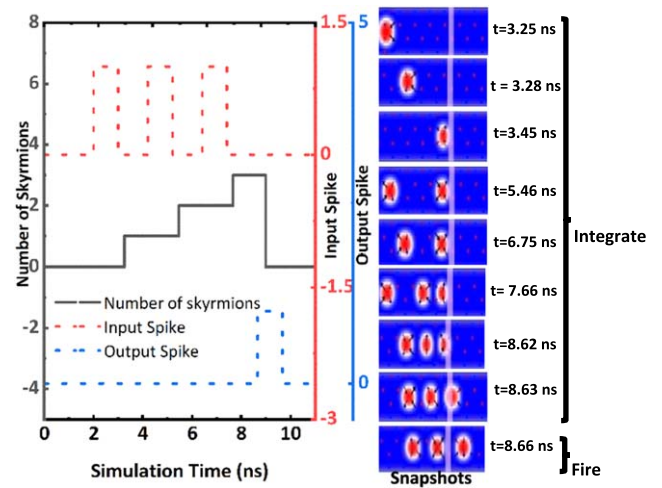


Figure 2. Micromagnetic simulation of proposed AFM skyrmion based neuron device with IF functionality.

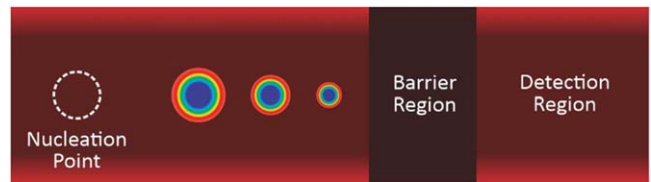


Figure 3. Schematic of proposed artificial neuron device.

number of skyrmions curve and, barrier cross delay is shown between the input spike and the output spike.

4. AFM skyrmion based artificial neuron device

4.1. Schematic of the proposed device

Figure 3 represents the schematic of the proposed AFM skyrmion-based artificial neuron device. This device has three primary components namely, nucleation point, barrier region, and a detection region. A nucleation point is a point where the skyrmions are initially created. The barrier region is the region with a higher magnetic anisotropy magnitude than other parts of nanotrack. The detection region is a region where the skyrmions are observed once they overcome the barrier region. The whole nanotrack has a fixed length of 856.06 nm and a width of 100.32 nm. A detection region has a length of about 277.55 nm.

4.2. Operation of the proposed device

A range of a number of skyrmions can be created on a nanotrack limited by the size of the device. An in-plane driving current is employed to drive a single skyrmion along the nanotrack from the nucleation point towards the detection region. The skyrmion’s ability to overcome the barrier is determined by an analysis of the forces acting on the skyrmions at the barrier. A repulsion force by the barrier acts on the skyrmion, opposing the driving force induced by the

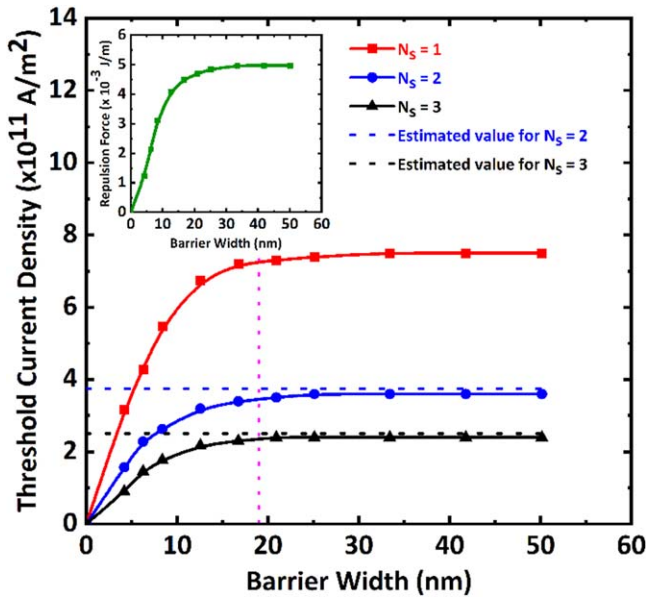


Figure 4. Plot of the threshold current density against the energy barrier width for devices with 1, 2, and 3 skyrmions. Here, N_s denotes the number of skyrmions on the track.

current. With an insufficient current, the skyrmion will be pinned at the barrier. Hence, an additional force is required to make the skyrmion overcome the barrier region. Thus, by nucleating additional skyrmions to form a chain of skyrmions, the first skyrmion experiences an additional force due to skyrmion-skyrmion repulsion acting between them. With a sufficient number of skyrmions, the first skyrmion is pushed past the barrier region and into the detection region. Once the skyrmion overcomes the barrier, the neuron fires an output signal and then reset it again. Using a triangular notch like structure at the ends of the nanotrack, the device can be reset so the skyrmions can be easily annihilated at the end.

5. Results and discussion

The threshold current density of the device with respect to the energy barrier width on the nanotrack is shown in figure 4. At first, it is observed that there is a smooth increase in the threshold current density for small barrier widths. Afterward, it gets saturated for large barrier width for any number of skyrmions on the track. This dependency of threshold current density on width is due to the finite skyrmion size. As the diameter of a magnetic skyrmion is finite, there is a dependency of repulsion force exerted by the barrier on its barrier width as shown by the inset of figure 4. The pink dotted line in figure 4 represents the skyrmion diameter on the nanotrack to portray the key idea intended here, which is the repulsion force becomes dependent on the barrier width on the scale of the size of skyrmion.

For current density less than $3.5 \times 10^{11} \text{ A m}^{-2}$, a single skyrmion on the track is not able to overcome the energy barrier width of 16.72 nm. By employing the chain of two skyrmions, the skyrmion is now able to overcome the barrier by the effect of skyrmion-skyrmion repulsion. However, for

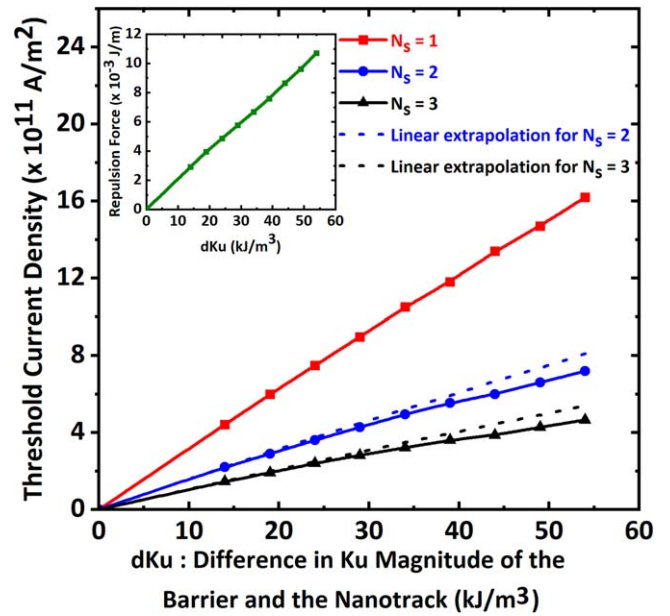


Figure 5. Plot of the threshold current density against the difference in anisotropy magnitude energy barrier and the nanotrack for devices with 1, 2, and 3 skyrmions. Here, N_s denotes the number of skyrmions on the track.

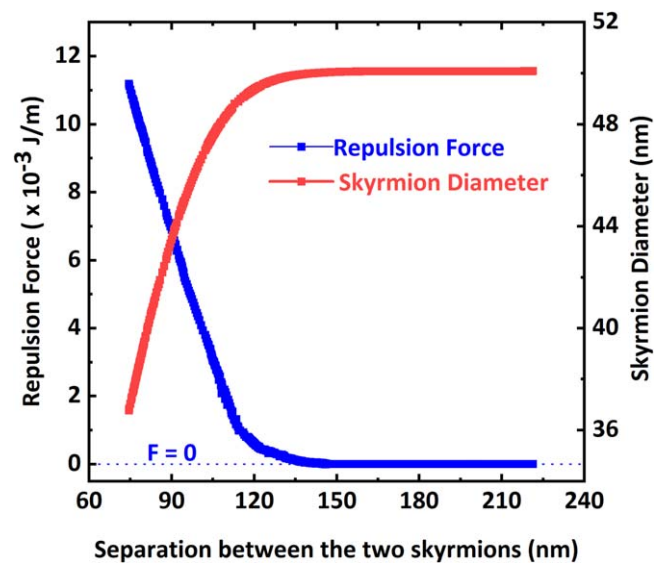


Figure 6. Variation of repulsion force between the two skyrmions and the skyrmion diameter with respect to the separation distance between the two skyrmions.

the chain of two skyrmions (with operating current density less than $2.4 \times 10^{11} \text{ A m}^{-2}$ and energy barrier of 41.80 nm), it will not overcome the barrier. The additional repulsive forces between the three skyrmions is a solution to force the skyrmion beyond the barrier.

Assuming the driving force due to current on skyrmions are constant, repulsion forces between the skyrmions are equal and opposite, and constant repulsive force exerted by the barrier. This accounts for the estimated value to be half ($3.75 \times 10^{11} \text{ A m}^{-2}$) and one-third ($2.5 \times 10^{11} \text{ A m}^{-2}$) for two and three skyrmions, respectively as compared to the single skyrmion on a track. It is

Table 2. Comparison of different neuron devices.

| S. no. | Neuron device | Energy consumption | Speed | Area |
|--------|---|--|--------------------------------------|--|
| 1 | CMOS based neurons [48–51] | Low (in pJ/spike) | Relatively low (in micro seconds) | Relatively high |
| 2 | FM skyrmion based neurons [26, 46, 47, 52, 53] | Low (in fJ/spike) | High | Low |
| 3 | AFM skyrmion based artificial neuron device (This work) | Estimated energy consumption is \sim fJ with current density of order 10^{11} A m ⁻² [46, 47] | High (2–2.5 ns) | Small size due to small skyrmion diameter (1–100 nm) |

noted that the current densities are marginally less (i.e. 3.5×10^{11} A m⁻² and 2.4×10^{11} A m⁻²) than the above-mentioned values. The decrease in threshold current density is likely to be due to a decrease in repulsive force by the barrier on the skyrmion as a result of a decrease in skyrmion diameter due to skyrmion-skyrmion repulsion. It is observed from figure 6 that the increased repulsive force between the two skyrmions result in decrease in the diameter of the skyrmion. Thus, tuning the device threshold with a greater number of skyrmions requires less current density.

The threshold current density with respect to magnetic anisotropy (K_u) in the energy barrier region is obtained for a fixed energy barrier width of 25.08 nm, as presented in figure 5. The threshold current density is computed for the range of dKu from 14 to 54 kJ m⁻³, where dKu is the difference in the K_u magnitude in the energy barrier region and that in the nanotrack. As observed in figure 5, there is a less than linear increase in the threshold current density with respect to the increase in K_u value of the high energy barrier region. The deviation from linearity at large anisotropy difference is more apparent for the case of 2 and 3 skyrmions.

The relation between the maximum repulsive force acting on the skyrmion due to the barrier against the change in dKu is illustrated in the inset of figure 5. The result supports the observed relation between the threshold current density and dKu .

Figure 6 shows the repulsion force as well as skyrmion diameter versus the separation between the two skyrmions. The deformation in skyrmion size due to skyrmion-skyrmion repulsion is very much significant. It can be seen that the repulsion force between the two skyrmions decreases dramatically from 0.017 to 0.0004 J m⁻¹ with an increase in inter-skyrmion distance from 74 to 124 nm. At the same time, skyrmion diameter is thus increased from 36.5 to 50 nm due to the repulsive forces between the two skyrmions. It can be observed that skyrmion-skyrmion repulsion is negligible for much higher inter-skyrmion separation as represented by $F = 0$ dotted line, thereby, keeping the skyrmion diameter constant.

The energy consumption of the proposed device is estimated to be in \sim femto Joules for the driving current density of order 10^{11} [46, 47]. The maximum transition time for the skyrmion to fire is in the range \sim 2–2.5 ns depending upon the barrier width and dKu .

In this section, we have explored the key device parameters and forces involved in the device's operation. Here, we provide an overview for optimizing the device for desired use. Firstly, as the device operation depends on the number of skyrmion on the nanotrack, its dimensions must be sufficient to

contain the maximum desired threshold number of skyrmions. Thereafter, the device's threshold may be lowered as required by operating at higher current density. On the other hand, the magnetic anisotropy barrier further enhances the tunability of the device to adjust the operating current density and optimize its power efficiency. At last, we have shown the comparison of CMOS and skyrmion-based neuron devices in table 2.

6. Conclusion

Most of the efforts have been targeted towards neuromorphic computing using FM skyrmions. However, FM skyrmions inherently have several limitations contrary to an AFM skyrmion that does not has stray fields and follows a straight trajectory due to mitigation of Magnus force. Hence, an antiferromagnetic skyrmion-based artificial neuron device is proposed based on the skyrmion-skyrmion repulsion effect. An integrate and fire (IF) functionality of the artificial neuron is demonstrated. The key device parameters and interactions that include inter-skyrmion repulsion on a nanotrack and skyrmion-barrier repulsion is investigated in order to show the tunability of the device. Furthermore, it is observed that these interactions account for the marginally lesser current densities for two and three skyrmions than the estimated values. The skyrmion compression is also observed, with an increase in inter-skyrmion repulsion. This device offers very low energy consumption and high processing speed, making it a potential candidate for the implementation of future skyrmionic devices in neuromorphic computing systems.

Acknowledgments

The authors are thankful to NTU-India connect program for sponsorship and support for carrying out this work. Also, the authors would like to thank the Dean of Resources and Alumni Affairs (DORA), Indian Institute of Technology, Roorkee for providing financial support.

Data availability statement

All data that support the findings of this study are included within the article (and any supplementary files).

ORCID iDs

Namita Bindal  <https://orcid.org/0000-0002-7252-4386>

Brajesh Kumar Kaushik  <https://orcid.org/0000-0002-6414-0032>

References

- [1] Nandakumar S R, Boybat I, Gallo M L, Eleftheriou E, Sebastian A and Rajendran B 2020 Experimental demonstration of supervised learning in spiking neural networks with phase-change memory synapses 2020 *Sci. Rep.* **10** 8080
- [2] Gao B et al 2014 Ultra-low three-dimensional oxide-based electronic synapses for implementation of robust high-accuracy neuromorphic computation *ACS Nano* **8** 7
- [3] Basu A, Ramakrishnan S, Petre C, Koziol S, Brink S and Hasler P E 2010 Neural dynamics in reconfigurable silicon *IEEE Trans. Biomed. Circuits Syst.* **4** 311
- [4] Zheng L, Shin S and Kang S S 2015 Memristor-based synapses and neurons for neuromorphic computing *IEEE Int. Symp. on Circuits and Systems (ISCAS) (Lisbon, Portugal, 24-27 May 2015)* (<https://doi.org/10.1109/ISCAS.2015.7168842>)
- [5] Suri M, Querlioz D, Bichler O, Palma G, Vianello E, Vuillaume D, Gamrat C and DeSalvo B 2013 Bioinspired stochastic computing using CBRAM synapses *IEEE Trans. Electron Devices* **60** 7
- [6] Gupta S, Kumar P, Paul T, Schaik A, Ghosh A and Thakur C S 2019 Low-power, CMOS-MoS₂ memtransistor based neuromorphic hybrid architecture for wake-up systems *Sci. Rep.* **9** 15624
- [7] Sengupta A and Roy K 2018 Neuromorphic computing enabled by physics of electron spins: prospects and perspectives *Appl. Phys. Express* **11** 030101
- [8] Sengupta A, Yogendra K and Roy K 2016 Spintronic devices for ultra-low power neuromorphic computation *IEEE Int. Symp. on Circuits and Systems (Montreal, QC, Canada, 22-25 May 2016)* (<https://doi.org/10.1109/ISCAS.2016.7527392>)
- [9] Grollier J, Querlioz D, Camsari K Y, Everschor-Sitte K, Fukami S and Stiles M D 2020 Neuromorphic spintronics *Nat. Electron.* **3** 360
- [10] Farakhani H, Tohid M, Farakhani S, Madsen J K and Moradi F 2018 A low-power high-speed spintronics based neuromorphic computing system using real-time tracking method *IEEE J. Emerging Sel. Top. Circuits Syst.* **8** 627
- [11] Zhang S and Tserkovnyak Y 2020 Antiferromagnet-based neuromorphics using dynamics of topological charges *Phys. Rev. Lett.* **125** 207202
- [12] Fert A, Cros V and Sampaio J 2013 Skyrmions on the track *Nat. Nanotechnol.* **8** 152
- [13] Jiang W, Chen G, Liu K, Zang J, Velthuis S G E and Hoffmann A 2017 Skyrmions in magnetic multilayers *Phys. Rep.* **704** 1–49
- [14] Yin G, Li Y, Kong L, Lake R K, Chien C L and Zang J 2016 Topological charge analysis of ultrafast single skyrmion creation *Phys. Rev. B* **93** 174403
- [15] Wang X S, Yuan H Y and Wang X R 2018 A theory on skyrmion size *Commun. Phys.* **1** 1
- [16] Woo S et al 2016 Observation of room-temperature magnetic skyrmions and their current-driven dynamics in ultrathin metallic ferromagnets *Nat. Mater.* **15** 501
- [17] Jonietz F 2010 Spin transfer torques in MnSi at ultralow current densities *Science* **330** 1648
- [18] Schulz T 2012 Emergent electrodynamics of skyrmions in a chiral magnet *Nat. Phys.* **8** 301
- [19] Yu X Z 2012 Skyrmion flow near room temperature in an ultralow current density *Nat. Commun.* **3** 988
- [20] Iwasaki J, Mochizuki M and Nagaosa N 2013 Universal current–velocity relation of skyrmion motion in chiral magnets *Nat. Commun.* **4** 1463
- [21] Iwasaki J, Mochizuki M and Nagaosa N 2013 Current-induced skyrmion dynamics in constricted geometries *Nat. Nanotechnol.* **8** 742
- [22] Sampaio J, Cros V, Rohart S, Thiaville A and Fert A 2013 Nucleation, stability and current-induced motion of isolated magnetic skyrmions in nanostructures *Nat. Nanotechnol.* **8** 839
- [23] Barker J and Tretiakov O A 2016 Static and dynamical properties of antiferromagnetic skyrmions in the presence of applied current and temperature *Phys. Rev. Lett.* **116** 147203
- [24] Yu G et al 2018 Room temperature skyrmions in antiferromagnetic based hetrostructures *Nano Lett.* **2** 980
- [25] Zhang X, Zhou Y and Ezawa M 2016 Antiferromagnetic skyrmion: stability, creation and manipulation *Sci. Rep.* **6** 24795
- [26] Li S, Kang W, Huang Y, Zhang X, Zhou Y and Zhao W 2017 Magnetic skyrmion based artificial neuron device *Nanotechnol.* **28** 31
- [27] Zhang X, Zhao G P, Fangohr H, Liu J P, Xia W X, Xia J and Morvan F J 2015 Skyrmion–skyrmion repulsion and skyrmion edge repulsions in skyrmion based- racetrack memory *Sci. Rep.* **5** 7643
- [28] Kang W, Huang Y, Zhang X, Zhou Y and Zhao W 2016 Skyrmion electronics: an overview and outlook *Proc. IEEE* **104** 10
- [29] Kang W, Huang Y, Zheng C, Lv W, Lei N, Zhang Y, Zhang X, Zhou Y and Zhao W 2016 Votage controlled magnetic skyrmion motion for racetrack memory *Sci. Rep.* **6** 23164
- [30] Song K M, Jeong J S, Pan B, Zhang X, Xia J, Cha S, Park T E, Kim K, Finizio S and Raabe J 2020 Skyrmion-based artificial synapses for neuromorphic computing *Nat. Electron.* **3** 148
- [31] Bhattacharya T, Li S, Huang Y, Kang W, Zhao W and Suri M 2019 Low power (1T1N) skyrmionic synapses for spiking neuromorphic computing *IEEE Access* **7** 1
- [32] Huang Y, Kang W, Zhang X, Zhou Y and Zhao W 2017 Magnetic skyrmion-based synaptic devices *Nanotechnology* **28** 08LT02
- [33] Chen R, Li C, Li Y, Miles J J, Indiveri G, Furber S, Pavlidis V F and Moutafis C 2020 Nanoscale room temperature multilayer skyrmionic synapse for deep spiking neural networks *Phys. Rev. Appl.* **14** 014096
- [34] Xia H, Jin C, Song C, Wang J and Liu Q 2017 Control and manipulation of antiferromagnetic skyrmions in racetrack *J. Appl. Phys.* **50** 17
- [35] Liang X, Zhao G, Shen L, Xia J, Zhao L, Zhang X and Zhou Y 2019 Dynamics of an antiferromagnetic skyrmion in a racetrack with a defect *Phys. Rev. B* **100** 14
- [36] Leliaert J, Dvornik M, Mulkers J, Clercq J D, Milosevic M V and Waeyenberge B V 2018 Fast micromagnetic simulations on GPU- recent advances made with MuMax3 *J. Appl. Phys.* **51** 123002
- [37] Nakatani Y, Uesaka Y and Hayashi N 1989 Direct solution of Landau–Lifshitz–Gilbert equation for micromagnetics *Japan. J. Appl. Phys.* **28** 12
- [38] Hopfield J J 1988 Artificial neural networks *IEEE Circuits Devices Magn.* **4** 5
- [39] Grollier J, Querlioz D and Stiles M D 2016 Spintronic nanodevices for bioinspired computing *Proc. IEEE* **104** 10
- [40] Izhikevich E M 2003 Simple model of spiking neurons *IEEE Trans. Neural Networks* **14** 6
- [41] Izhikevich E M 2004 Which model to use for cortical spiking neurons? *IEEE Trans. Neural Networks* **15** 5

- [42] Gerstner W and Kistler W M 2002 *Spiking Neuron Models: Single Neurons, Populations, Plasticity* 1st edn (Cambridge: Cambridge University Press) (<https://doi.org/10.1017/CBO9780511815706>)
- [43] Abbott L F 1999 Lapicque's introduction of the integrate-and-fire model neuron (1907) *Brain Res. Bull.* **50**
- [44] Burkitt A N 2006 A review of integrate and fire neuron model: homogenous synaptic input *Biol. Cybern.* **95** 1
- [45] Uhrig R E 1995 Introduction to artificial neural networks *IEEE Conf. on Industrial Electronics (IECON) (Orlando, USA, 6-10 Nov. 1995)* (<https://doi.org/10.1109/IECON.1995.483329>)
- [46] He Z and Fan D 2017 A tunable magnetic skyrmion neuron cluster for energy efficient artificial neural network *Design, Automation & Test in Europe Conf. & Exhibition (DATE) (Lausanne Switzerland, 27-31 March 2017)* (<https://doi.org/10.23919/DATE.2017.7927015>)
- [47] Chen X, Kang W, Zhu D, Zhang X, Lei N, Zhang Y, Zhou Y and Zhao W 2018 A compact skyrmionic leaky-integrate-fire spiking neuron device *Nanoscale* **10** 13
- [48] Azghadi M R *et al* 2020 Complementary metal oxide semiconductor and memristive hardware for neuromorphic computing *Adv. Intell. Syst.* **2** 1900189
- [49] Wu X, Saxena V, Zhu K and Balagopal S 2015 A CMOS spiking neuron for brain-inspired neural networks with resistive synapses and *in situ* learning *IEEE Trans. Circuit Theory II* **62** 1088
- [50] Cruz-Albrecht J, Yung M W and Srinivasa N 2012 Energy-efficient neuron, synapse and STDP integrated circuits *IEEE Trans. Biomed. Circuits Syst.* **6** 3
- [51] Indiveri G *et al* 2011 Neuromorphic silicon neuron circuits *Front. Neurosci.* **5** 73
- [52] Liang X, Zhang X, Xia J, Ezawa M, Zhao Y, Zhao G and Zhou Y 2020 A spiking neuron constructed by the skyrmion-based spin torque nano-oscillator *Appl. Phys. Lett.* **116** 122402
- [53] Azam M A, Bhattacharya D, Querlioz D and Atulasimha J 2018 Resonate and fire neuron with fixed magnetic skyrmions *J. Appl. Phys.* **124** 152122